

# The Influence of Different Structure of Magnetic Modulation Ring on the Torque Performance of Coaxial Magnetic Gear

Jungang Wang<sup>1, \*</sup>, Shuirui Xu<sup>1</sup>, Aiguo Ouyang<sup>1</sup>, and Ruina Mo<sup>2</sup>

**Abstract**—In coaxial magnetic gear (CMG), magnetic modulation ring is composed of a modulator and a connecting bridge. The torque performance of the magnetic gear is affected by the different structures of the magnetic modulation ring. In this paper, fifteen different kinds of magnetic modulation rings with different structures are proposed; they consist of three different shapes of modulators and five different locations of connection bridges. By using the two-dimensional finite element method (FEM), the magnetic flux density, magnetic line distribution, static torque, and steady-state torque of the CMG with different structures of magnetic modulation ring are analyzed. The results show that the innermost bridge has the least effect on the torque and torque ripple of the CMG, while the outermost bridge has the opposite effect. The torque capacity of the circular modulator and arc modulator is higher than that of the square modulator, and the circular modulator helps to reduce the inner torque ripple, while the square modulator helps to reduce the outer torque ripple. This paper can provide some references for the design of the magnetic modulation ring.

## 1. INTRODUCTION

Compared with mechanical gears, magnetic gears can be driven in a non-contact manner, which reduces the additional maintenance on the gears and reduces the noise when the gears are working [1]. The topological structure of the first generation of magnetic gears is similar to that of mechanical helical gears. However, due to the defects of its structure, the utilization rate of permanent magnets is low, which makes the torque density far lower than that of mechanical gears [2, 3]. In order to solve this problem, CMG was first proposed in 2001. Compared with the earlier parallel axis topology, the concentric structure significantly improves the utilization of permanent magnets of a magnetic gear [4, 5]. Based on the principle of magnetic field modulation, a modulator is introduced to modulate the air-gap magnetic field. This modulation can make the number of pole pairs of the maximum harmonic field in the air gap equal to that of the permanent magnet. Meanwhile, the rotation of the harmonic field can be synchronized with the permanent magnet, thus generating stable working torque between the rotors [6–8]. Compared with mechanical gear, CMG has the advantages of non-contact transmission, low noise, maintenance-free operation, and inherent overload protection [9, 10]. Also, CMG usually has a higher torque density than the motor, so when coaxial magnetic gear and motor are integrated, the torque density of the whole system can be improved [11–13]. With the development of the new energy industry, magnetic gear composite motor topology has been proposed due to the excellent characteristics of magnetic gear and is considered to be used in wind power generation and pure electric vehicles [14, 15].

The modulator is a crucial component of a coaxial magnetic gear. The design of the modulator will directly affect the torque performance of the magnetic gear [16]. The conventional modulators are composed of independent silicon steel sheets. However, this structure is not easy to process and install,

---

*Received 27 August 2020, Accepted 14 October 2020, Scheduled 22 October 2020*

\* Corresponding author: Jungang Wang (sduhys@163.com).

<sup>1</sup> School of Mechatronics & Vehicle Engineering, East China Jiaotong University, Nanchang, China. <sup>2</sup> School of Science, East China Jiaotong University, Nanchang, China.

and does not guarantee sufficient mechanical strength [17]. To reduce complexity and enhance reliability, [18] proposed a full-layer magnetic modulation ring composed of a modulator and a connection bridge. Ref. [19] used the finite element method to analyze the performance of the prototype for modulators of different shapes; the results showed that the circular modulator had advantages in reducing the torque fluctuation and eddy current loss of the permanent magnet. In [20], three kinds of modulators with different structures were proposed, and the proposed structures were discussed from the aspects of torque performance and loss of permanent magnets. Ref. [21] proposed a novel dual-flux-modulator coaxial magnetic gear. The outer rotor permanent magnet adopted a spoked structure, and an auxiliary magnetic modulation ring was introduced in the outermost layer. Through theoretical and experimental analysis, it was proved that the torque performance of the structure and the utilization ratio of the permanent magnet are greatly improved. In [22], the distribution of torque on the magnetic modulation ring was analyzed in detail. The Maxwell stress tensor method was used for theoretical derivation, and the torque distribution on each surface of different connection bridges was obtained. Based on the simulation analysis and experiment, some suggestions were given on the mechanical strength and torque transfer capability of the bridge. At present, there are many types of researches on conventional modulators, but there are relatively few researches on the magnetic modulator ring with a full-layer structure, especially considering the shape of the modulator and the position of the connecting bridge at the same time. Therefore, in view of the transmission performance of a coaxial magnetic gear, it is necessary to study the magnetic modulation ring with different structures.

In this paper, we respectively propose the radial and tangential flux density expressions of air gap before and after introducing a modulator, and the principle of magnetic field modulation is explained in detail. Three different shapes of circular, arc, and square modulators are combined with five different positions of the connecting bridge: inner bridge, outer bridge, middle bridge, innermost bridge, and outermost bridge. Based on the two-dimensional numerical analysis, by using the nonlinear finite element analysis method, the magnetic flux density, magnetic flux distribution, static torque, and steady-state torque of the conventional modulator and the proposed full-layer magnetic modulation ring are analyzed and compared, respectively.

## 2. PRINCIPLE OF MAGNETIC FIELD MODULATION

Figure 1 shows the topology structure of a conventional CMG. The permanent magnets of the rotor are attached to the corresponding rotor iron yoke. Rotor permanent magnets are radially magnetized, and adjacent magnets are magnetized in opposite directions. The arrangement of the modulators shown in the figure is an ideal arrangement, which means that the adjacent modulators are independent of each other and are not connected through a connection bridge. In order to prevent the energy loss caused by eddy current, the modulator is made of silicon steel sheets superimposed axially, and insulation coating exists between adjacent sheets.

When the modulator does not exist, the radial and tangential flux densities generated by any permanent magnetic rotor at radial distance  $r$  can be expressed as,

$$B_r^0(r, \theta) = \sum_{m=1,3,5\dots} b_{rm}(r) \cos[mp(\theta - \omega_r t) + mp\theta_0] \quad (1)$$

$$B_\theta^0(r, \theta) = \sum_{m=1,3,5\dots} b_{\theta m}(r) \sin[mp(\theta - \omega_r t) + mp\theta_1] \quad (2)$$

where  $m$  is the harmonic order;  $p$  is the number of pole pairs of the permanent magnet of the rotor;  $\omega_r$  is the angular velocity of the rotor;  $\theta$  and  $\theta_1$  are the radial and tangential initial angles of the magnetic flux density distribution, respectively;  $b_{rm}$  and  $b_{\theta m}$  are Fourier coefficient.

After the introduction of the modulator, the magnetic field excited by the permanent magnet of the inner or outer rotor can be modulated due to the existence of the modulator, so that abundant spatial harmonics can be generated in the two air gaps around the modulator. The radial and tangential modulation functions of the modulator can be expressed as,

$$\lambda_r(r, \theta) = \lambda_{r0}(r) + \sum_{j=1,2,3,\dots} \lambda_{rj}(r) \cos(jn_s(\theta - \omega_r t)) \quad (3)$$

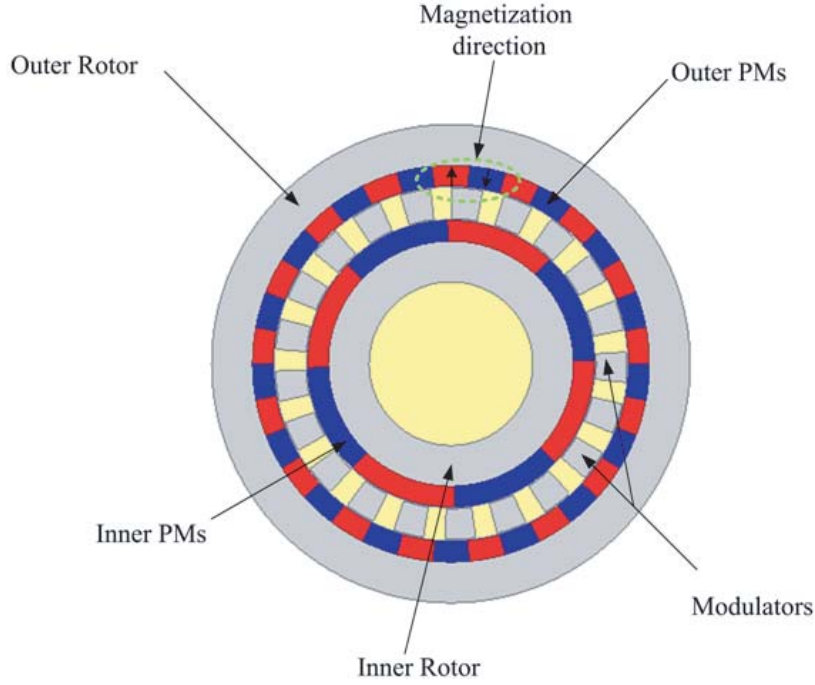


**Figure 1.** Topological structure of conventional CMG.

$$\lambda_{\theta}(r, \theta) = \lambda_{\theta 0}(r) + \sum_{j=1,2,3,\dots} \lambda_{\theta j}(r) \sin(jn_s(\theta - \omega_r t)) \quad (4)$$

where  $j$  is the harmonic order,  $n_s$  the number of modulators, and  $\lambda_{r0}$ ,  $\lambda_{\theta 0}$ ,  $\lambda_{rj}$ ,  $\lambda_{\theta j}$  are Fourier coefficients. It can be concluded that the radial and tangential magnetic flux densities of the air gap modulated by the modulator are,

$$B_r(r, \theta) = B_r^0(r, \theta) \cdot \lambda_r(r, \theta) \quad (5)$$

$$B_{\theta}(r, \theta) = B_{\theta}^0(r, \theta) \cdot \lambda_{\theta}(r, \theta) \quad (6)$$

The modulator mainly affects the inner and outer air-gap magnetic fields, so that the inner and outer air-gap magnetic fields are effectively coupled to generate the corresponding torque. It can be known from Eqs. (5) and (6) that the number of pole pairs and rotation of space harmonics excited by any permanent magnet rotor speed satisfy the following expression,

$$P_{m,k} = |mp + kn_s| \quad (7)$$

$$\Omega_{m,k} = \frac{mp}{mp + kn_s} \Omega_r + \frac{kn_s}{mp + kn_s} \Omega_s \quad (8)$$

where  $m = 1, 3, 5 \dots$ ,  $k = 0, \pm 1, \pm 2 \dots$ ,  $P$  is the pole pair number of the inner or outer rotor permanent magnets.  $m$ ,  $\Omega_{m,k}$  are the angular velocities of space harmonics;  $\Omega_r$  is the angular velocities of the inner or outer rotors; and  $\Omega_s$  is the angular velocity of the modulator. It can be seen from Eq. (8) that when  $k = 0$ , that is, the magnetic modulation ring does not exist, the angular velocity of the spatial harmonic  $\Omega_{m,k}$  is equal to the angular velocity  $\Omega_r$  of the inner or outer rotor. When torque transmission is at different speeds,  $k$  should not be 0. When  $m = 1$ ,  $k = -1$ , the asynchronous space harmonics are the highest. The number of pole pairs of the rotor permanent magnet must satisfy the following relationship,

$$P_{in} + P_{out} = n_s \quad (9)$$

where  $P_{in}$  and  $P_{out}$  are the pole pairs of the inner and outer rotor permanent magnets, respectively. In this case, the magnetic gear transmission ratio can be expressed as,

$$G_r = \frac{p_{out}}{p_{in}} \quad (10)$$

### 3. SIMULATION ANALYSIS

#### 3.1. Different Structure of Magnetic Modulation Ring

Figure 2 shows the different topological structures of the magnetic modulation ring. It can be seen from Figure 2 that three modulators of different shapes are proposed, among which design 1 is a circular modulator, design 2 an arc modulator, and design 3 a square modulator. Each modulator corresponds to five connection bridges, inner bridge, outer bridge, middle bridge, innermost bridge, and outermost bridge. To make the proposed structure comparable, the area of the grey modulator is equal in all designs, and the thickness of the connection bridge remains unchanged at 3 mm.

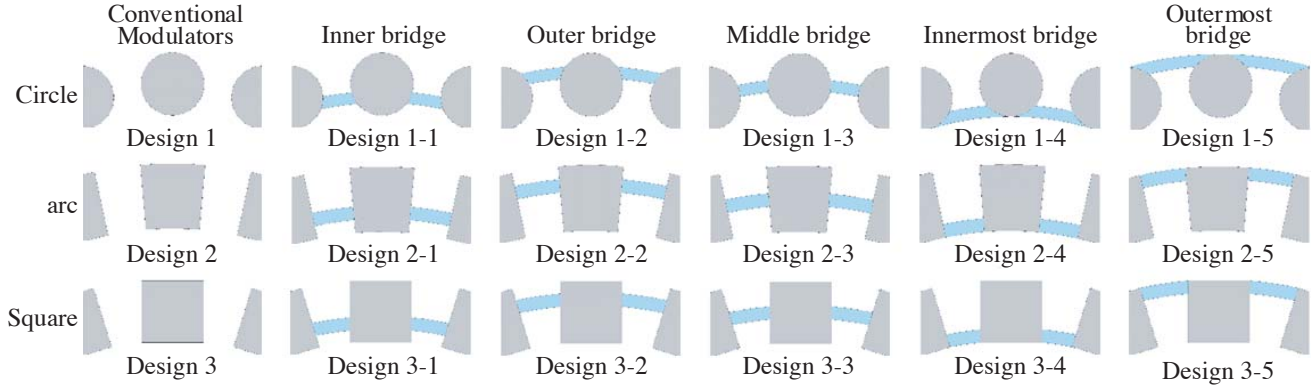


**Figure 2.** Different structures of the magnetic modulation ring.

Figure 3 shows the prototype when design 2-3 is installed. In the proposed prototype, the material of the permanent magnets is NdFeB; the remanence of permanent magnets is 1.21 T; and the coercivity of permanent magnets is 875 kA/m. The materials used for the inner and outer rotor yokes are iron, and the magnetic modulation ring is composed of silicon steel sheets with good magnetic permeability. In order to ensure the comparability, only the structural parameters of the magnetic modulation ring are different, and other structural parameters of the prototype are the same. Table 1 shows the parameters of the proposed prototype.

**Table 1.** Structural parameters of the prototype.

Parameter	Value
Number of inner pole-pairs	4
Number of outer pole-pairs	17
Number of flux modulators	21
Thickness of interconnecting bridge	3 mm
Thickness of magnets	10 mm
Diameter of inner rotor	70 mm
Diameter of outer rotor	117 mm
The axial length	40 mm
Gear ratio	17/4
Remanence of PMs	1.21 T

#### 3.2. Magnetic Field Analysis

For the coaxial magnetic gear with magnetic field modulation, the number of permanent magnet pole pairs on the inner rotor is generally not equal to that on the outer rotor. As a medium to transfer torque

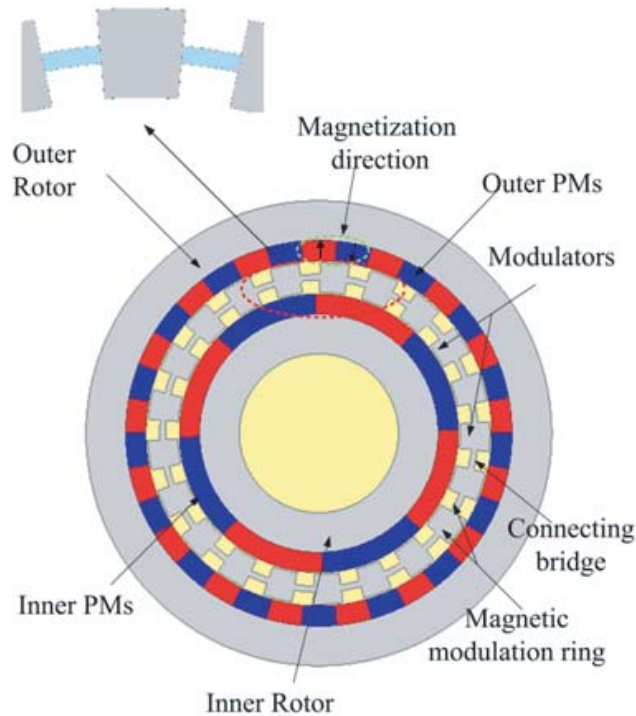


**Figure 3.** Proposed prototype.

between inner and outer rotors, the magnetic modulation ring generates abundant spatial harmonics between inner and outer air gaps through non-uniform magnetic field paths. The space harmonics with the same pole pair number and speed are effectively coupled, which achieves stable torque transmission between the inner and outer rotors. The inner and outer air gaps are the key to torque formation. The magnetic field distribution in the air gap will directly affect the transmission performance of magnetic gears.

Figure 4 shows the magnetic flux density distribution of the prototype with eight different magnetic modulation rings. As can be seen from Figure 4, there is no magnetic saturation phenomenon in the prototype under each magnetic modulation ring. According to Figures 4(a), 4(b), and 4(c), when there is no connection bridge, the maximum flux density is generated at the edge of the modulator. It can be seen from Figure 4(d)–Figure 4(h) that when the connection bridge is installed, regardless of the shape of the modulator, the magnetic flux density tends to be more concentrated at the connection bridge of each magnetic modulation ring.

It can be seen from the distribution of magnetic induction lines that regardless of the presence or absence of a connecting bridge, most of the magnetic induction lines at the highest magnetic flux density do not pass through the modulator to effectively couple with the corresponding permanent magnets, but with the adjacent permanent magnet through the modulator. Therefore, most of the magnetic inductance lines at the highest flux density are not helpful to the working torque generation of the prototype. Comparing Figure 4(d), Figure 4(e), and Figure 4(f), it can be seen that the outer rotor has a large number of pole pairs, resulting in a short pole moment, so compared with the innermost bridge and middle bridge, adding the outermost connecting bridge can make it easier for the magnetic induction lines to close on adjacent magnetic poles, which can affect the torque performance of the prototype.

Figure 5 shows the inner air gap magnetic flux density distribution for design 1, design 2, and design 3. From Figure 5, we can see the effect of the four pairs of pole-pair inner rotor permanent magnets. Although there are many magnetic field spikes due to the presence of the modulator, four complete magnetic field cycles can still be observed. It can be observed that the amplitude of the magnetic flux density using the arc modulator is higher than the other two modulators. By performing

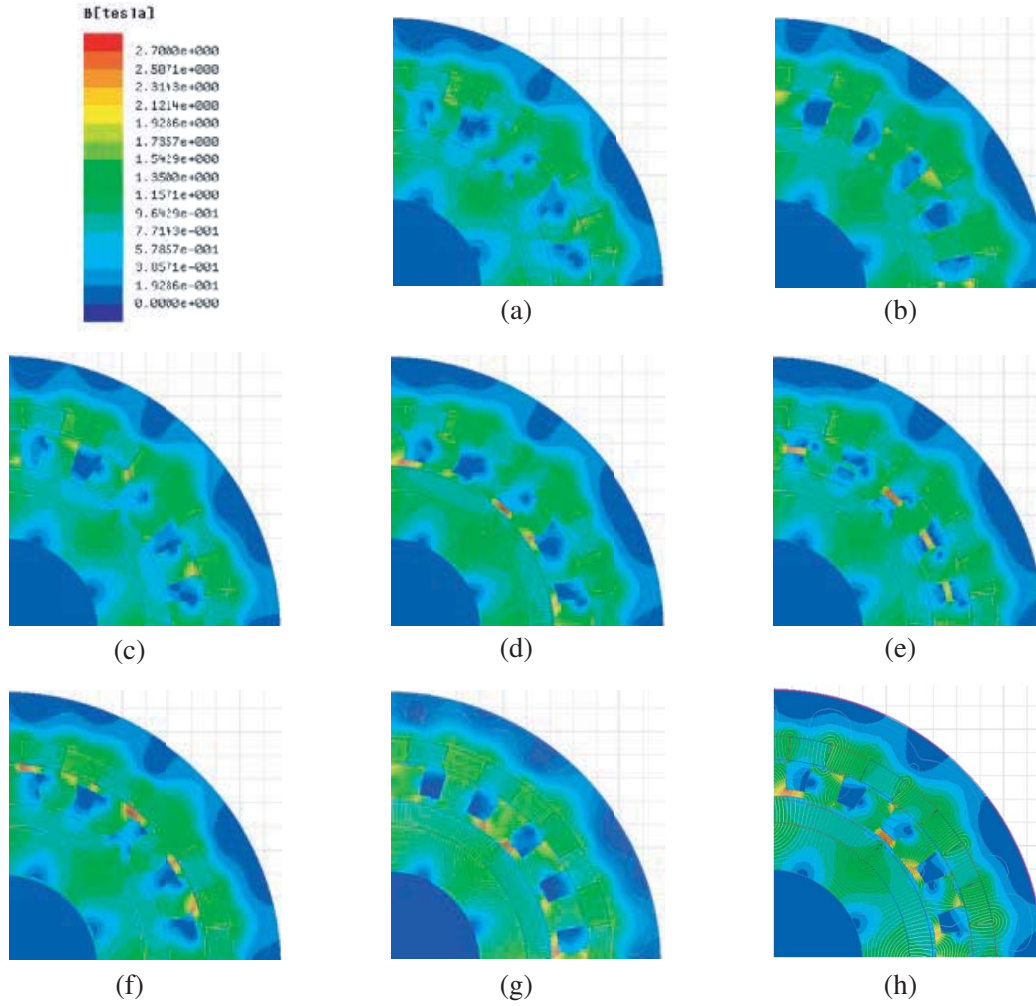


**Figure 4.** Magnetic flux density distribution. (a) Design 1; (b) Design 2; (c) Design 3; (d) Design 1-4; (e) Design 1-3; (f) Design 1-5; (g) Design 2-4; (h) Design 3-4.

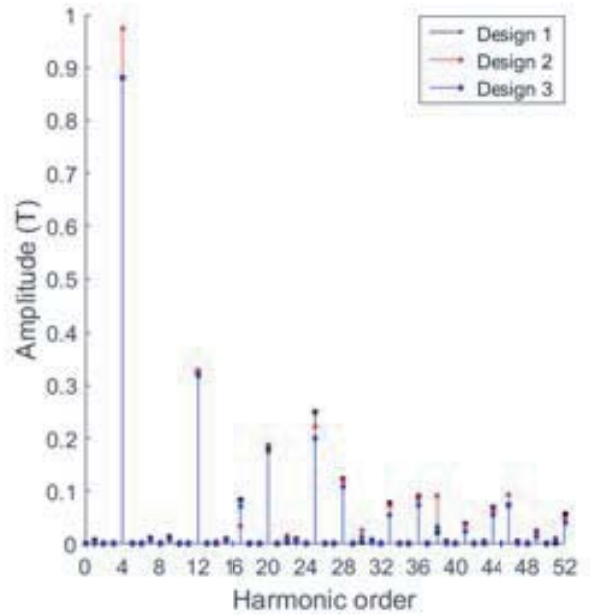
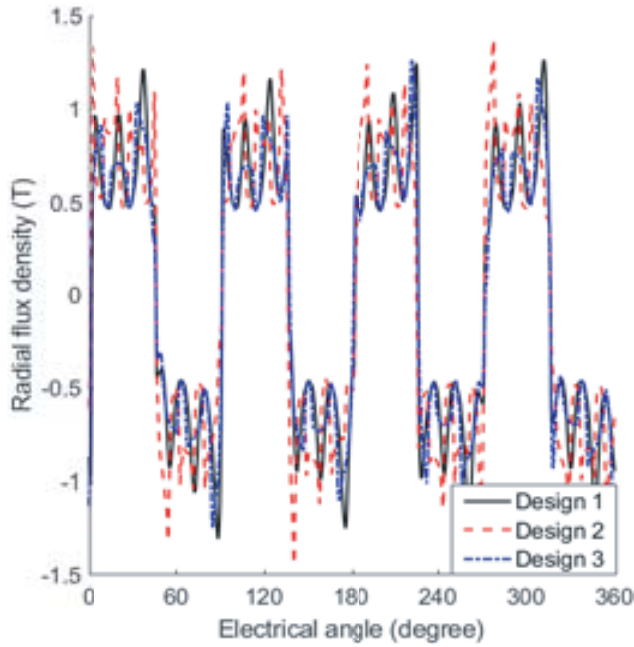
a fast Fourier transform on the radial magnetic flux density waveform of the inner air gap under each design, the spatial harmonic spectrum of the radial magnetic flux density component of the inner air gap under each design can be obtained.

Figure 6 shows the spatial harmonic spectrum. It can be seen that under the action of the modulator, the inner air gap magnetic field introduces a large number of harmonics. It mainly includes 4, 12, 17, 20, 25, 28, 33, 36, 38, 41, and 46 magnetic field harmonics, of which the 4th harmonic has the largest amplitude, which is the highest harmonic that generates transmitted torque. We can see that the 4th harmonic amplitude of the arc modulator is higher than that of the other two modulators without the connection bridge.

The sinusoidal property of inner air gap magnetic density can be quantitatively represented by the harmonic distortion rate of each designed spatial harmonic spectrum, and the harmonic distortion rate (THD) is defined as,

$$THD = \sqrt{\frac{\sum_{i=2}^{\infty} B_i^2}{B_a^2}} \times 100\% \quad (11)$$

where  $B_a$  is the magnetic flux density amplitude of the fundamental wave, and  $B_i$  is the magnetic flux density amplitude of each order harmonic ( $i = 1, 2, 3 \dots$ ).



**Figure 5.** Radial flux density distribution of inner air gap.

**Figure 6.** Spatial harmonic spectrum.

Table 2 shows the internal air gap THD under each design. It can be seen that the introduction of the connection bridge can reduce the harmonic distortion rate of air gap to some extent. When the shape of the modulator is the same, the gap harmonic distortion rate of the innermost connection bridge is the lowest, while the gap harmonic distortion rate of the outermost connection bridge is the highest. Under the same shape of the modulator, the innermost bridge can improve the air gap magnetic density waveform, improve the sine degree of the air gap magnetic density, and the combination of the arc modulator and the innermost bridge can make the inner air gap magnetic density waveform have better sine.

**Table 2.** THD of inner air gap.

Design	1	1-1	1-2	1-3	1-4	1-5
THD (%)	58.80	51.93	53.86	53.63	47.99	55.23
Design	2	2-1	2-2	2-3	2-4	2-5
THD (%)	52.71	46.34	48.23	47.78	39.66	49.88
Design	3	3-1	3-2	3-3	3-4	3-5
THD (%)	52.72	45.21	46.25	45.90	41.45	47.69

### 3.3. Static Torque Curve

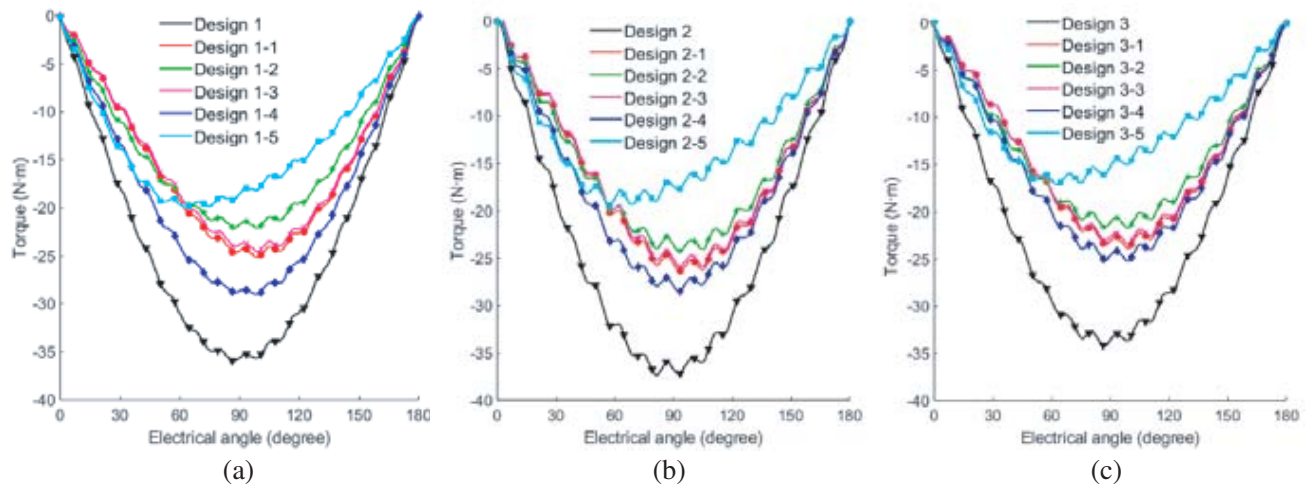
The static torque of the magnetic gear is an essential indicator for measuring its transmission performance. If the applied load torque exceeds the peak torque, the inner and outer rotors of the magnetic gear will no longer be driven according to the predetermined transmission ratio. Therefore, the static torque of magnetic gear directly determines its load capacity. The static torque of magnetic gear can be obtained by the Maxwell tensor method [23],

$$T_i = \frac{L_{ef}}{\mu_0} \int_0^{2\pi} B_n B_t d\theta \tag{12}$$

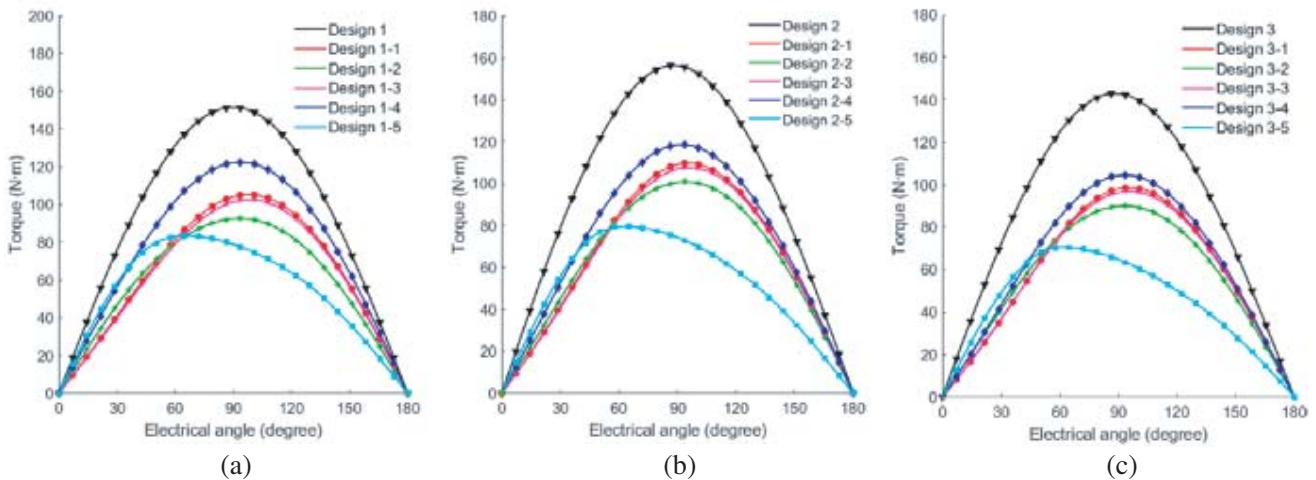
where  $L_{ef}$  is the axial length of the magnetic gear;  $\mu_0$  is the vacuum permeability;  $B_n$  and  $B_t$  are the radial and tangential flux density components at radius  $r$ , respectively.

Figure 7 and Figure 8 are static torque curves of the inner and outer rotors, respectively. Comparing Figure 7 and Figure 8, it can be seen that the static torque curves of the inner and outer rotors have a good sine degree in a half cycle, and the directions of the inner and outer torques are opposite. Except for the outermost bridge, the static torque curves of other designs all reach the amplitude at an electrical angle about 90 degrees. It can be seen from Figure 7 and Figure 8 that the peak torque generated by designs 1, 2, and 3 in three modulators of different shapes is the largest, and the torque performance of the prototype decreases to some extent after the connection bridge is installed. Designs 1-4, 2-4, and 3-4 with the innermost connection bridge have the smallest decrease, while designs 1-5, 2-5, and 3-5 with the outermost connection bridge have the most significant decrease. The torque performances of the circular and arc modulators are higher than that of the square modulator when the position of the bridge is the same.

Table 3 shows the specific values of the peak torque of the outer rotor for each design. Based on the peak torques at designs 1, 2, and 3 respectively, Designs 1-4, 1-5, 2-4, 2-5, 3-4, 3-5 are 80.8%, 55.2%, 75.5%, 51.0%, 73.6%, 49.2% of the reference value respectively. It can be concluded that the static peak torques of connection bridges with different positions are very different, and the



**Figure 7.** Static torque curve of inner rotor. (a) Circular; (b) arc; (c) square.



**Figure 8.** Static torque curve of outer rotor. (a) Circular; (b) arc; (c) square.

**Table 3.** Peak torque of outer rotor.

Design	1	1-1	1-2	1-3	1-4	1-5
Value (N · m)	151.5	105.2	92.4	102.8	122.4	83.6
Design	2	2-1	2-2	2-3	2-4	2-5
Value (N · m)	156.2	109.6	100.8	107.6	118.4	79.6
Design	3	3-1	3-2	3-3	3-4	3-5
Value (N · m)	143.0	98.8	90.0	97.2	105.2	70.4

innermost connection bridges are usually more than 20% higher than the outermost connection bridges. Besides, the combination of the circular modulator and the innermost connection bridges has the most considerable peak torque in all the designs with added connection bridges.

### 3.4. Steady-State Torque Curve

Figures 9, 10, and 11 show the steady-state torque curve at the maximum torque position for each design. It can be seen from the figure that the torque of the inner and outer rotors hardly changes with the change of the electrical angle, which means that a very stable working torque is formed on the inner and outer rotors. In the same design, the direction of the internal and external torques of the prototype are opposite, and the torque ripple of the inner rotor is significantly higher than that of the outer rotor. With the different positions of the connecting bridges, the magnitude of the steady-state torque of each design in order from high to low is no bridge, innermost bridge, inner bridge, middle bridge, outer bridge, and outermost bridge. When the position of the connecting bridge is the same, but the shape of the modulator is different, for the convenience of observation, the steady-state torque curves of 1-4, 2-4, and 3-4 are designed in comparison. It can be seen that the steady-state torque size is as follows from the height to the bottom: the circular modulator, arc modulator, and square modulator.

In order to quantitatively compare the torque fluctuation under the steady-state operation of

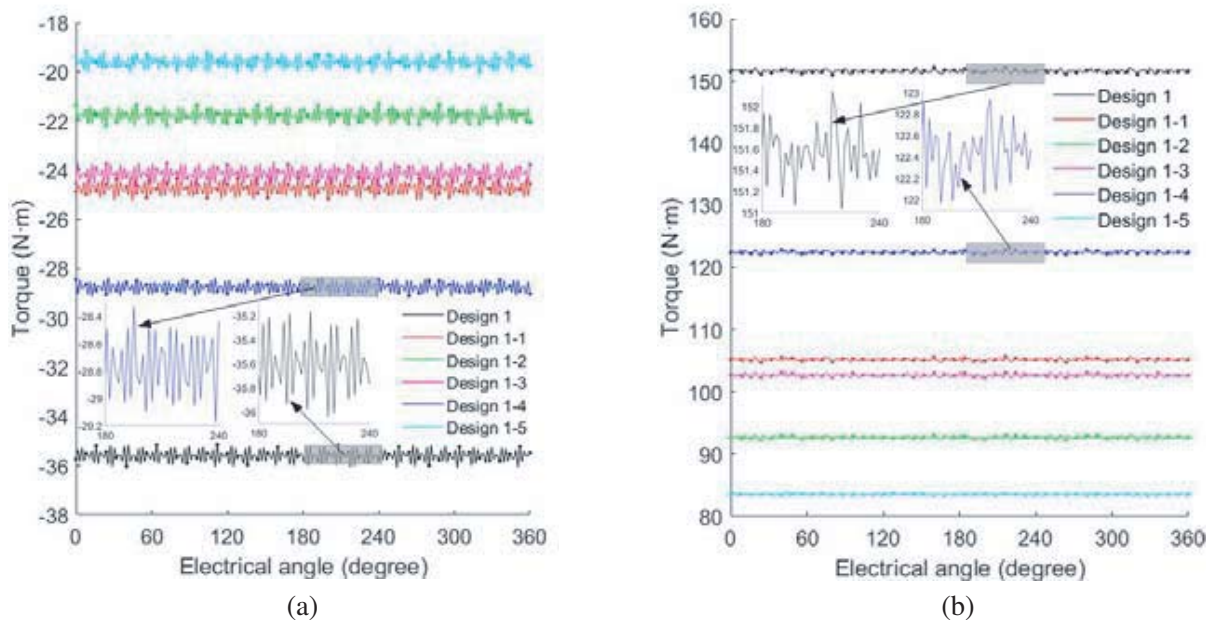


**Figure 9.** Steady-state torque curve with Circular modulator. (a) Inner rotor; (b) outer rotor.

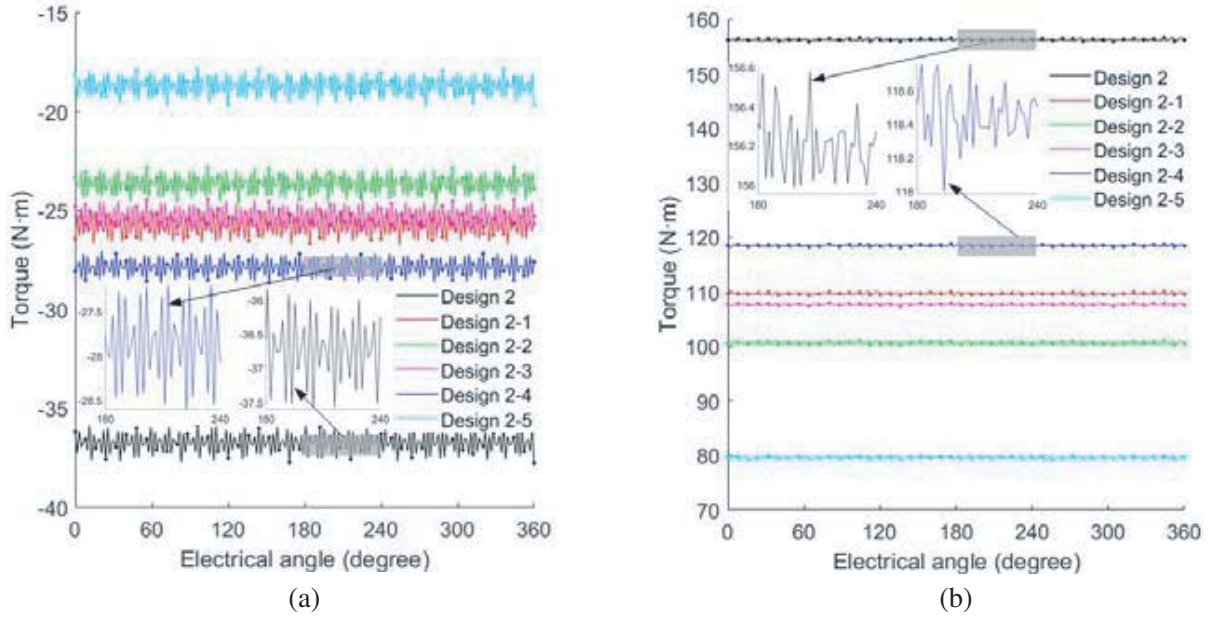


**Figure 10.** Steady-state torque curve with arc modulator. (a) Inner rotor; (b) outer rotor.

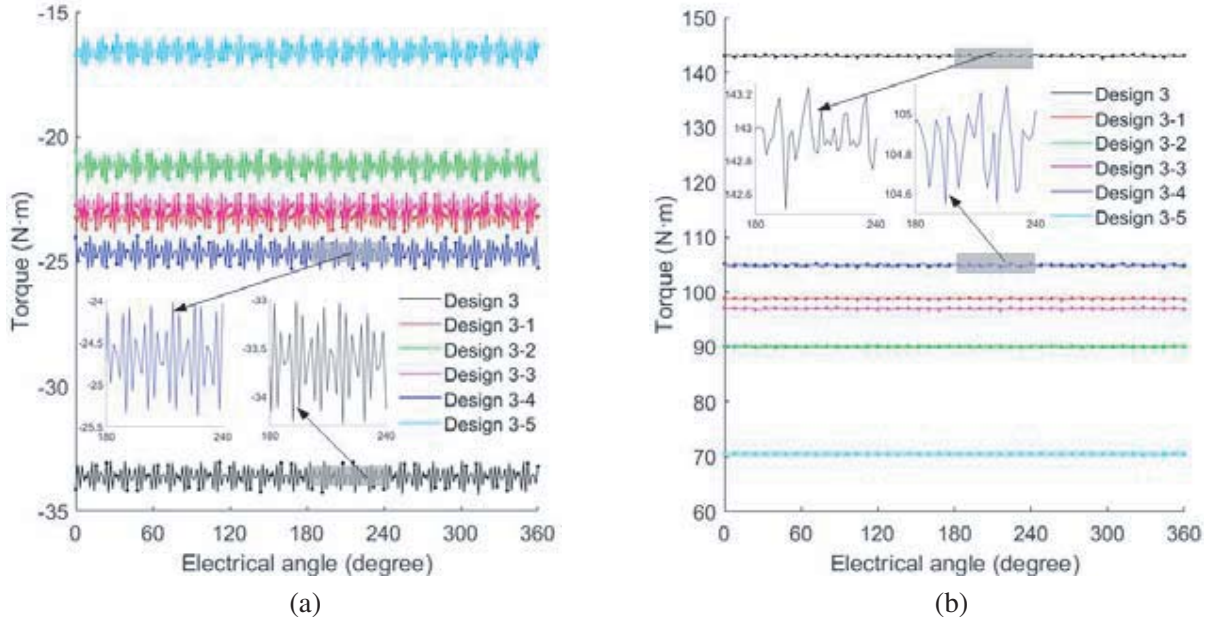


**Figure 11.** Steady-state torque curve with square modulator. (a) Inner rotor; (b) outer rotor.

individual designs, torque ripple  $K_{ripple}$  is defined as,

$$K_{ripple} = \frac{T_{\max} - T_{\min}}{T_{\text{avg}}} \times 100\% \quad (13)$$

where  $T_{\max}$ ,  $T_{\min}$ , and  $T_{\text{avg}}$  are the maximum, minimum, and average values of steady-state torque, respectively. By calculating the data obtained in Figures 9, 10, and 11, the magnitude of the torque ripple of the inner and outer rotors under various designs can be quantitatively derived.

**Table 4.** Average torque and torque ripple.

	$T_{avg}$ of inner rotor (N·m)	$T_{avg}$ of outer rotor (N·m)	$K_{ripple}$ of inner rotor	$K_{ripple}$ of outer rotor
Design 1	35.62	151.58	2.66%	0.88%
Design 1-1	24.74	105.16	4.06%	1.02%
Design 1-2	21.77	92.64	4.31%	1.23%
Design 1-3	24.13	102.68	4.03%	1.06%
Design 1-4	28.75	122.44	2.95%	0.79%
Design 1-5	19.62	83.48	4.80%	1.02%
Design 2	36.80	156.28	5.20%	0.54%
Design 2-1	25.82	109.72	7.32%	0.81%
Design 2-2	23.78	100.64	8.19%	0.85%
Design 2-3	25.41	107.72	7.67%	0.75%
Design 2-4	27.84	118.48	5.92%	0.81%
Design 2-5	18.85	79.56	10.31%	1.13%
Design 3	33.66	142.93	4.09%	0.59%
Design 3-1	23.24	98.80	5.72%	0.61%
Design 3-2	21.20	90.00	6.48%	0.71%
Design 3-3	22.83	97.00	5.75%	0.60%
Design 3-4	24.67	104.92	5.75%	0.69%
Design 3-5	16.56	70.48	7.94%	0.38%

Table 4 shows the average torque and torque ripple on the inner and outer rotors of each design. It can be concluded that the ratio of the average torque of the outer rotor to the average torque of the inner rotor is always approximately equal to the transmission ratio of the prototype 17 : 4, regardless of the combination mode of the modulator and connection bridge. By comparing the torque ripple of the inner rotor with design 1, design 2, and design 3, it can be concluded that the torque ripple on the inner rotors can be intensified to some extent by adding the connection bridge. The addition of the innermost connection bridge will only slightly increase the inner torque ripple of the prototype, while the addition of the outermost connection bridge can seriously aggravate the inner torque ripple of the prototype. In addition, when the position of the connecting bridge is the same, the inner and outer torque ripples caused by the modulators of different shapes are different. It can be seen from the comparison that the inner torque ripple of the circular modulator is the smallest, and the square modulator is more excellent in reducing the outer torque ripple.

#### 4. CONCLUSION

In this paper, three different shapes of circular, arc, and square modulators are combined with five different positions of the connecting bridge: inner bridge, outer bridge, middle bridge, innermost bridge, and outermost bridge. Based on two-dimensional numerical analysis, using nonlinear finite element analysis methods, the magnetic flux density, magnetic line distribution, static torque, and steady-state torque of the prototype with different structures of magnetic modulation ring are analyzed and compared with the performance of no connection bridge. The simulation results can be obtained,

1. When connecting bridges are installed between modulators, the highest flux density is generally concentrated at the connecting bridges of various magnetic modulation rings. Most of the magnetic inductance lines with the highest flux density are not effectively coupled with the corresponding permanent magnets, but with the adjacent permanent magnets. Therefore, most of the magnetic

inductance lines at the highest flux density do not contribute to the working torque of the magnetic gear. Since the pole moment of the permanent magnet is shorter due to a large number of poles in the outer rotor, the adoption of the outermost connection bridge will make the magnetic induction line easier to close at the adjacent magnetic poles, thus affecting the torque performance of the magnetic gear.

2. Compared with the non-connecting bridge, the installation of the connecting bridge will reduce the torque capacity of the magnetic gear. Based on the peak torque, when there is no connecting bridge, the decrease of torque caused by using the innermost bridge is less than that caused by the outermost bridge. When the position of the connecting bridge is fixed, the torque capacity of the circular or arc modulator is higher than that of the square modulator. In terms of torque capacity, the combination of the circular modulator and the innermost bridge results in the smallest reduction in torque capacity.

3. By comparing with the internal torque ripple of design 1, design 2, and design 3, it can be concluded that the installation of the connecting bridge will aggravate the inner torque ripple of the magnetic gear. The inner torque ripples caused by the connecting bridges at different positions are different. The inner torque ripple caused by the innermost bridge is the smallest, while the inner torque ripple caused by the outermost bridge is the largest. When the position of the connecting bridge is fixed, the use of a circular modulator helps reduce inner torque ripple, while the use of a square modulator helps reduce outer torque ripple.

## ACKNOWLEDGMENT

This work was supported by the National Natural Science Foundation of China (Grant No. 51765020).

## REFERENCES

1. Atallah, K., S. D. Calverley, and D. Howe, "Design, analysis and realisation of a high-performance magnetic gear," *IEE Proceedings — Electric Power Applications*, Vol. 151, No. 2, 135, 2004.
2. Tsurumoto, K. and S. Kikuchi, "A new magnetic gear using permanent magnet," *IEEE T. Magn.*, Vol. 23, No. 5, 3622–3624, 1987.
3. Yao, Y. D., D. R. Huang, S. M. Lin, and S. J. Wang, "Theoretical computations of the magnetic coupling between magnetic gears," *IEEE T. Magn.*, Vol. 32, No. 3, 710–713, 1996.
4. Filippini, M. and P. Alotto, "Coaxial magnetic gear design and optimization," *IEEE T. Ind. Electron.*, Vol. 64, No. 12, 9934–9942, 2017.
5. Tsai, M. and C. Huang, "Development of a variable-inertia device with a magnetic planetary gearbox," *IEEE/ASME Transactions on Mechatronics*, Vol. 16, No. 6, 1120–1128, 2011.
6. Gerber, S. and R. Wang, "Design and evaluation of a magnetically geared PM machine," *IEEE T. Magn.*, Vol. 51, No. 8, 1–10, 2015.
7. Zhu, X., L. Chen, L. Quan, Y. Sun, W. Hua, and Z. Wang, "A new magnetic-planetary-geared permanent magnet brushless machine for hybrid electric vehicle," *IEEE T. Magn.*, Vol. 48, No. 11, 4642–4645, 2012.
8. Jing, L., T. Zhang, Y. Gao, R. Qu, Y. Huang, and T. Ben, "A novel HTS modulated coaxial magnetic gear with eccentric structure and halbach arrays," *IEEE T. Appl. Supercon.*, Vol. 29, No. 5, 1–5, 2019.
9. Rasmussen, P. O., T. O. Andersen, F. T. Jorgensen, and O. Nielsen, "Development of a high-performance magnetic gear," *IEEE T. Ind. Appl.*, Vol. 41, No. 3, 764–770, 2005.
10. Uppalapati, K. K., M. D. Calvin, J. D. Wright, J. Pitchard, W. B. Williams, and J. Z. Bird, "A Magnetic Gearbox with an Active Region Torque Density of 239 N·m/L," *IEEE T. Ind. Appl.*, Vol. 54, No. 2, 1331–1338, 2018.
11. Dragan, R. S., R. E. Clark, E. K. Hussain, K. Atallah, and M. Odavic, "Magnetically geared pseudo direct drive for safety critical applications," *IEEE T. Ind. Appl.*, Vol. 55, No. 2, 1239–1249, 2019.
12. Iwasaki, N., M. Kitamura, and Y. Enomoto, "Optimal design of permanent magnet motor with magnetic gear and prototype verification," *Electr. Eng. Jpn.*, Vol. 194, No. 1, 60–69, 2016.

13. Peng, S., W. N. Fu, and S. L. Ho, "A novel high torque-density triple-permanent-magnet-excited magnetic gear," *IEEE T. Magn.*, Vol. 50, No. 11, 1–4, 2014.
14. Wang, R. and S. Gerber, "Magnetically geared wind generator technologies: Opportunities and challenges," *Appl. Energ.*, Vol. 136, 817–826, 2014.
15. Zhu, X., L. Chen, L. Quan, Y. Sun, W. Hua, and Z. Wang, "A new magnetic-planetary-geared permanent magnet brushless machine for hybrid electric vehicle," *IEEE T. Magn.*, Vol. 48, No. 11, 4642–4645, 2012.
16. Liu, X., Y. Zhao, Z. Chen, D. Luo, and S. Huang, "Multi-objective robust optimization for a dual-flux-modulator coaxial magnetic gear," *IEEE T. Magn.*, Vol. 55, No. 7, 1–8, 2019.
17. Wang, Y., M. Filippini, N. Bianchi, and P. Alotto, "A review on magnetic gears: Topologies, computational models, and design aspects," *IEEE T. Ind. Appl.*, Vol. 55, No. 5, 4557–4566, 2019.
18. Li, X., M. Cheng, and Y. Wang, "Analysis, design and experimental verification of a coaxial magnetic gear using stationary permanent-magnet ring," *IET Electr. Power App.*, Vol. 12, No. 2, 231–238, 2018.
19. Kim, S. J., E. Park, S. Jung, and Y. Kim, "Transfer torque performance comparison in coaxial magnetic gears with different flux-modulator shapes," *IEEE T. Magn.*, Vol. 53, No. 6, 1–4, 2017.
20. Abdelhamid, D. Z. and A. M. Knight, "The effect of modulating ring design on magnetic gear torque," *IEEE T. Magn.*, Vol. 53, No. 11, 1–4, 2017.
21. Zhang, X., X. Liu, and Z. Chen, "A novel dual-flux-modulator coaxial magnetic gear for high torque capability," *IEEE T. Energy Conver.*, Vol. 33, No. 2, 682–691, 2018.
22. Jian, L., Z. Deng, Y. Shi, J. Wei, and C. C. Chan, "The mechanism how coaxial magnetic gear transmits magnetic torques between its two rotors: Detailed analysis of torque distribution on modulating ring," *IEEE/ASME Transactions on Mechatronics*, Vol. 24, No. 2, 763–773, 2019.
23. Amrhein, M. and P. T. Krein, "Force calculation in 3-D magnetic equivalent circuit networks with a Maxwell stress tensor," *IEEE T. Energy Conver.*, Vol. 24, No. 3, 587–593, 2009.